Uniaxial Nonlocal Formulation for Geometric Nonlinearity–Induced Necking and Buckling Localization in a Steel Bar

Subodh Kolwankar, S.M.ASCE[1]; Amit Kanvinde, M.ASCE[2];
Maha Kenawy, S.M.ASCE[3]; and Sashi Kunnath, F.ASCE[4]

Abstract: A nonlocal formulation with the potential to mitigate mesh dependence in fiber models for steel elements is presented. The formulation addresses two common modes of localization in prismatic steel bars: tension necking and compression buckling. These modes are induced by geometric nonlinearity, unlike those addressed by previous nonlocal formulations that focus on localization induced by material softening. Continuum finite element (FE) simulations are conducted to provide benchmark data for development as well as validation of the nonlocal formulation. The nonlocal formulation is implemented through a one-dimensional (1D) line-element-based structural model and has the following features: (1) a uniaxial stress-strain relationship with softening; (2) a length scale representing the necking or buckling process; (3) a volume-averaged nonlocal strain measure that incorporates this length scale; and (4) an imperfection pattern. For both necking and buckling, the nonlocal formulation successfully mitigates mesh dependence shown by the local models, implying that it can reproduce softening load deformation response accurately regardless of mesh discretization. Additionally, comparison to FE benchmark data indicates that the nonlocal formulation is able to characterize the strains inside the localized zone. This latter observation has important implications for simulation of fracture or fatigue that originates in zones of localized strains, such as during cyclic buckling of rebar or local buckling-induced fracture in rolled shapes. Limitations of the study are outlined, identifying challenges for incorporation into fiber models for beam-column elements. **DOI:** [10.1061/(ASCE)ST.1943-541X.0001827](). © *2017 American Society of Civil Engineers.*

Author keywords: Fiber models; Localization; Nonlocal formulations; Frame elements; Metal and composite structures.

Introduction

Accurate simulation of extreme-limit states in structures subjected to earthquake or blast has long been a major focus of the structural engineering and mechanics research communities. These limit states are associated with local or global instability such as tension necking, local buckling and fracture in steel frame structures and concrete crushing, loss of confinement and reinforcing bar buckling in reinforced concrete structures, and the accompanying loss of component strength leading to structural collapse. These phenomena may be simulated through methods developed over nearly five decades within the area of nonlinear structural mechanics, including: (1) phenomenological spring or hinge models calibrated to component load-deformation response [see Jin and El-Tawil (2005), or Dides and de la Llera (2005) for a comprehensive review]; (2) fiber models that simulate cross-sectional behavior by aggregating uniaxial material response (Spacone et al. 1996); and (3) continuum finite element (FE) models that directly simulate

processes such as necking and buckling, along with multiaxial constitutive response. Landmark guidance documents (FEMA 2009; NIST 2009) have facilitated the use of these methods, with the ultimate objective of simulating extreme limit states such as collapse. Continuum FE simulations are generally considered unfeasible for modeling frames in professional practice. Consequently, practitioners as well as researchers rely on line-element-based frame simulations using concentrated hinge/spring models or fiber formulations. The hinge models are computationally efficient but require calibration to component-specific tests and cannot be easily generalized to untested components. Moreover, they cannot conveniently simulate spread of plasticity (through the member length) or axial force-moment (P-M) interaction. Fiber models, which are a subset of line-element models, simulate these effects but are compromised when softening and associated localization (concentration of strain over a small zone) occurs in the member. In steel elements, localization is triggered by tension necking or local buckling such as flange local buckling or buckling of a reinforcing bar, whereas in concrete members, it may be triggered by material softening (e.g., crushing). In fiber models, these behaviors are represented through a softening constitutive relationship used in conjunction with Gauss integration points or element discretization along the length of the member. Fig. 1 illustrates this approach schematically, indicating the physical processes that control localization, and their idealizations within a fiber-based approach. Although commonly used for frame simulation, this approach is problematic for two reasons:

1. When softening constitutive models are used, the simulated post-peak response is nonobjective [Fig. 1(b)]; that is, it is highly sensitive to discretization (number of Gauss points or mesh size—Ibrahimbegovic 2009). Thus, to reproduce physical or experimental response, the softening properties (negative

[1]Graduate Research Assistant, Dept. of Civil and Environmental Engineering, Univ. of California, Davis, CA 95616.

[2]Professor, Dept. of Civil and Environmental Engineering, Univ. of California, Davis, CA 95616 (corresponding author). E-mail: kanvinde@ucdavis.edu

[3]Graduate Research Assistant, Dept. of Civil and Environmental Engineering, Univ. of California, Davis, CA 95616.

[4]Professor, Dept. of Civil and Environmental Engineering, Univ. of California, Davis, CA 95616.
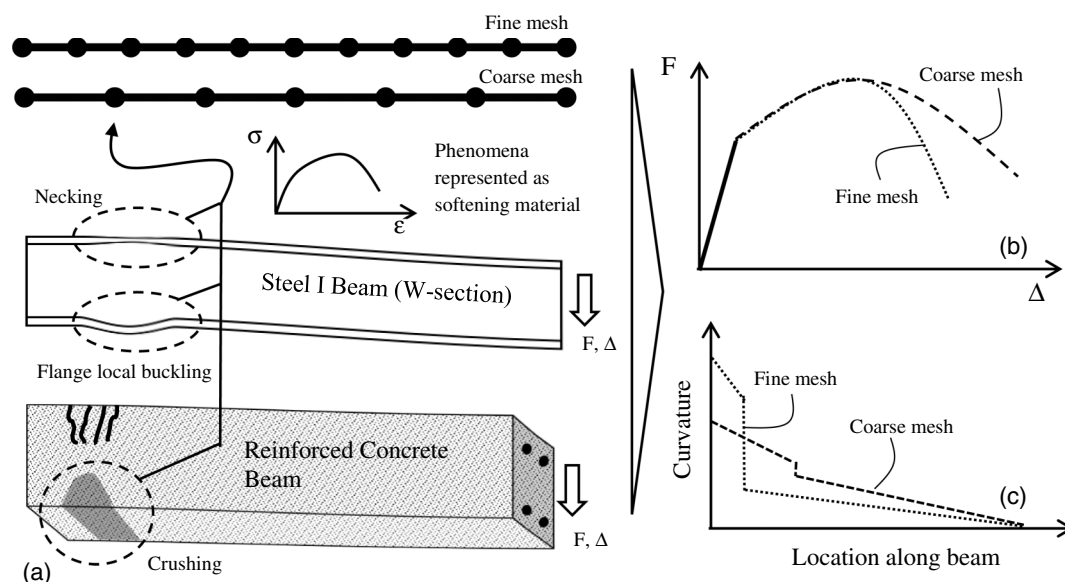
Fig. 1. Fiber-based simulation of localization processes through softening constitutive models

stiffness) must be selected in an ad hoc manner in concert with the mesh. Strategies to mitigate this nonobjectivity range from empirical guidelines to energy-based methods that establish relationships between mesh size and softening stiffness (Coleman and Spacone 2001; Pugh et al. 2015). Numerous studies (Ibarra and Krawinkler 2005; Lignos and Krawinkler 2011) indicate that structural collapse is especially sensitive to the post-peak stiffness, underscoring the need to simulate it accurately.

2. The strategies described here have focused on reinforced concrete elements, in which softening and localization is constitutive in nature. Contrastingly, in steel members, the softening response arises from geometric nonlinearity associated with necking or local buckling rather than from material softening. In representing these through a uniaxial constitutive relationship, the fiber approach disregards the length scale (e.g., wavelength of local buckle; Fig. 1) that controls softening. As a consequence, the simulated strains within the localized zone are meaningless since they are normalized by a mesh-dependent gauge length. Fig. 1(c) shows an entirely dissimilar curvature distributions for different mesh sizes. This is particularly problematic if these curvatures or strains are to be used for other purposes, such as fracture or fatigue prediction. Specifically, fracture in the localized zone such as at the local buckle in a cyclically loaded brace or beam (Fig. 2) is controlled by these localized strains.

Therefore, predicting this type of fracture with the fiber approach necessitates empirical "fudge-factors," which cannot be easily generalized across different cross sections. Previous research (Fell et al. 2010; Uriz 2005; Huang 2009) has focused on developing such factors, recognizing that direct simulation of localized continuum strains, and subsequently fracture or fatigue, is not tractable within conventional fiber approaches. Some researchers (e.g., Krishnan and Hall 2006) have combined fiber with plastic hinge approaches to mitigate mesh-dependence through a finite-length plastic hinge while retaining attractive features (P-M interaction) of the fiber approach. However, these approaches presuppose the location of localization.

To address these issues, this paper presents a nonlocal formulation for simulation of necking and buckling controlled softening in a steel bar. This formulation embeds a length scale into the uniaxial constitutive relationship which relies on a nonlocal strain field determined by averaging the conventional strain over a volume defined by this length scale. Thus far, nonlocal approaches have been used to eliminate mesh-dependence for softening material constitutive response in which the length scale is associated with internal morphological features, such as aggregate size in concrete. These approaches are well studied (Jirásek and Rolshoven 2003; Engelen et al. 2003) and have been applied to various situations, including shear banding in geomaterials (Shuttle and Smith 1988), crushing

Fig. 2. Local buckling-induced strain amplification within tubular brace leading to fracture (reprinted from Fell 2008, with permission)

in concrete (Bazant 1976), and softening due to porosity increase ahead of advancing crack tips in steel (Enakoutsa et al. 2007). In large measure, these formulations address continuum simulations; several researchers have studied these approaches for frame elements as well. This includes work by Armero and Ehrlich (2004, 2006) and Marante et al. (2004), among others. Research by Valipour and Foster (2009) implemented nonlocal formulations to simulate concrete crushing in fiber-based frame elements. Even more recently, Sideris and Salehi (2016), and Zhang et al. (2014) implemented gradient-based formulations for frame elements. However, all these implementations share the following features: (1) they are primarily focused on localization due to material (typically concrete) softening; and (2) their main concern is the mitigation of mesh-dependence rather than simulation of strains within the localized zone. The nonlocal formulation presented in this paper is novel in that it simulates localization due to *geometric nonlinearity*, and (in addition to mitigating mesh dependence) it is also able to characterize the strains within the localized zone. The formulation addresses a cylindrical bar, which despite its simplicity exhibits geometric nonlinear localization in tension as well as compression. In concentrating on this geometrically simple condition, the purpose is to develop foundational concepts for nonlocal modeling of geometric softening in steel elements, which may subsequently be incorporated into fiber models that simulate full cross-sectional response. More specifically, the objectives and the scope of this paper are as follows:

1. To present a uniaxial nonlocal formulation for a steel bar subject to necking-induced localization in tension, and buckling-induced localization in compression. The formulation is distinguished by (1) an explicit length scale, reflecting necking/buckling phenomena; (2) mitigation of mesh dependence; and (3) resulting strain distributions (within the localized zone) that are consistent with those obtained from continuum FE simulations, such that they may be used in downstream simulation and assessment of fracture and fatigue.
2. To develop, calibrate, and validate this formulation using continuum FE simulations that directly simulate various phenomena responsible for localization and examine challenges for application to more realistic settings where localization may occur over a cross-section, and/or under-reversed cyclic loading.

Conventionally, it is understood that material damage or degradation is responsible for localization. Where computational resources are available, these phenomena may be simulated directly through mesomechanical or micromechanical simulations (e.g., through void cell simulation for steel—Faleskog et al. 1998, or lattice models for concrete—Kim et al. 2013). However, in the vast majority of cases where continuum mechanics-based simulation is the only option, this must be simulated as constitutive softening. This gives rise to mesh-dependence, which must then be mitigated through techniques such as nonlocal formulation to reintroduce material-specific length scales into the solution. The phenomena (necking and buckling) addressed in this paper are different in the sense that they, unlike material damage, can be conveniently simulated through continuum mechanics. However, they are not simulated directly in the predominant framework for structural modeling, which relies on frame elements. In this framework, buckling and necking are represented as constitutive softening (as standard procedure), giving rise to tactical issues of mesh-dependence that are strikingly similar to those observed when material damage is simulated constitutively. It is important to emphasize that this mesh dependence and localization is not at the material level but merely an artifact of the manner in which the strain is represented in a uniaxial fiber model. Accordingly, this research expediently adapts a methodology usually used for

constitutive softening induced localization to address necking or buckling induced localization.

Problem Definition

The nonlocal formulation described here is informed by (1) the physical underpinnings of the uniaxial bar problem; and (2) parametric FE simulations of the uniaxial bar to recover quantitative data and insights regarding the localization processes, the load deformation response, and strain distributions. This section defines the problem in terms of its physics and analytical derivations, as a precursor to the FE simulations discussed in the next section. The subsequent section integrates observations from these two sections to present the nonlocal formulation. Note that necking under tension and buckling under compression are governed by entirely different physical processes, and they may be treated as distinct problems, although they both feature a cylindrical bar. Following this, the discussion of their governing physics (in this section), as well as their FE simulation, and finally the formulation are presented separately.

Necking in a Cylindrical Steel Bar

The tension necking response of a bar is well studied in literature (Bridgman 1964); only a brief overview is provided here. Fig. 3(a) schematically illustrates a cylindrical bar of cross-sectional area A_0 and arbitrary length subjected to tension, whereas Figs. 3(b and c) illustrate the longitudinal strain distribution and the load deformation
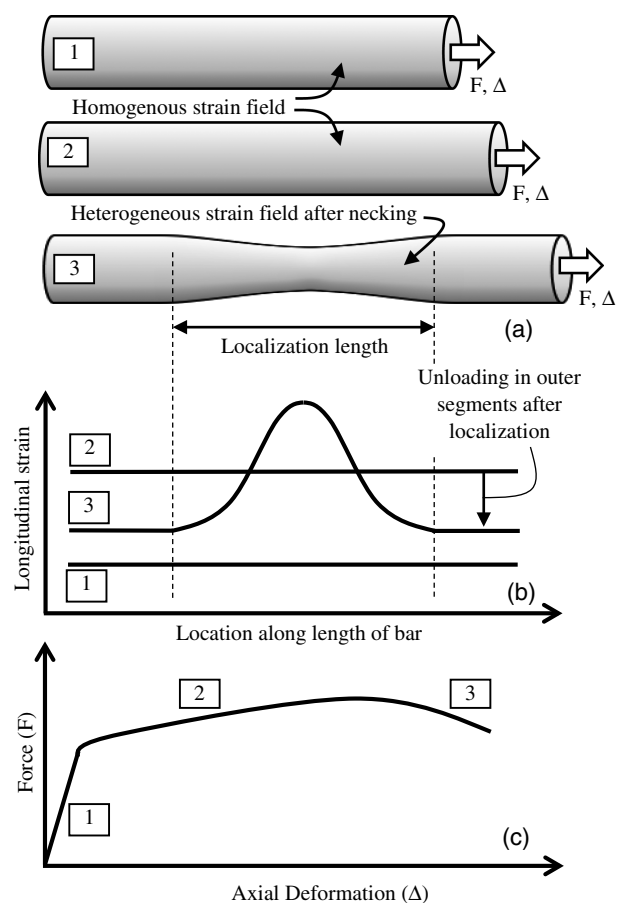

Fig. 3. Necking localization in a tension bar: (a) schematic illustration; (b) evolution of strain distribution; (c) load-deformation curve

response. After an initial phase of elastic loading, the bar begins to undergo yielding. During this phase, the bar is strained homogeneously, with increasing stress due to material strain hardening. This continues until the ultimate strength of the material is reached, corresponding to a peak point in the load deformation curve [Fig. 3(c)]. From a physical standpoint, this occurs when the stress increase due to strain hardening cannot compensate for the decrease in cross-sectional area due to straining. The well-known Considère (1885) criterion expresses this condition mathematically:

$$\sigma = \frac{d\sigma}{d\varepsilon} \qquad (1)$$

In Eq. (1), σ and ε = longitudinal true stress and strain respectively, implying that the peak point is attained when the true stress equals the slope of the tangent to the true stress-strain curve. Eq. (1) indicates an instability, such that after this criterion is satisfied, an imperfection (e.g., a cross section with smaller area) results in increase of strain at this cross section with an accompanying decrease in force, leading to softening response. The reduction of cross-sectional area in the vicinity of this weaker section forms a neck [Fig. 3(a)]. The ensuing evolution of the deformation (and stress) field is controlled by complex interactions of the evolving three-dimensional (3D) neck geometry (and associated nonhomogeneous strain fields) with the multiaxial constitutive properties of the steel material. Due to these interactions, at any instant, a segment of the bar is loading, such that the net longitudinal strain across it is increasing, whereas the remainder of the bar unloads elastically. From the perspective of this study, the pertinent observations are:
1. The strain corresponding to the initiation of necking instability may be determined analytically from the Considère criterion.
2. The post-peak softening is the result of complex interactions involving the change of neck geometry (cross-section as well as longitudinal profile) under a nonhomogeneous and triaxial stress state, coupled with constitutive hardening of the material itself. Accurate simulation of this post-necking response is not tractable analytically (i.e., in a closed form), and requires numerical solution, as pointed out by Needleman (1972) and subsequently Norris et al. (1978).
3. During this softening response, the neck represents a physical length scale due to 3D geometry changes, which may be interpreted in a manner similar to morphological length scales that control post-peak response in softening materials. This length scale controls the softening response, as well as the strain field internal to the neck.

Buckling and Localization of a Prismatic Steel Bar

The post-buckling response of prismatic elements has been studied in various settings, including buckling of bracing elements (Ikeda and Mahin 1986; Fell et al. 2010) and reinforcing steel (Zong et al. 2014). Figs. 4(a and b) schematically illustrate the post-buckling response of a solid prismatic bar fixed at the ends and the corresponding load deformation curve. While the elastic buckling strength of the bar may be predicted through the Euler formula, which assumes a perfectly straight, elastic member, it cannot be used to characterize either the strength or the post-buckling response for bars that yield and are geometrically imperfect. For L/d, ratios less than 20 (which are the focus of the formulations in this paper, with possible applications to reinforcing bars, and extensions to flange local buckling), the compressive strength is controlled by inelastic buckling or yielding and is equal to $F_y A_0$ of the bar (Zong et al. 2014). For larger L/d ratios, the strength is controlled by the bar slenderness, as well as imperfections
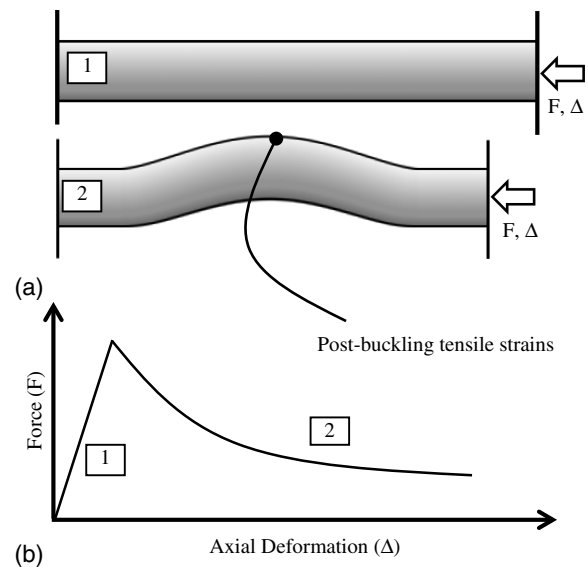

Fig. 4. Buckling localization in fixed-fixed bar: (a) schematic illustration; (b) load-deformation curve

and residual stresses, if present. After buckling or yielding, the response falls on a spectrum depending on bar slenderness. Highly squat bars ($L/d < 5$) exhibit hardening after yield, with no discernible peak point; these are less interesting from the perspective of this study. Bars with higher slenderness ($8 < L/d < 20$), which are of primary interest in this study, exhibit a peak point and softening post-buckling response, as shown in Fig. 4(b). The softening post-buckling response shown in Fig. 4 is associated with bending of the bar, and induces tensile strain at the extreme fiber at the points of maximum curvature [Fig. 4(a)]. Buckling-induced tensile strain causes low-cycle fatigue and fracture of reinforcing bars, as well as steel braces and beams that undergo local buckling. In the context of this study, the relevant points are (1) the yield or compressive strength, as well as post-buckling load-deformation response may be characterized based on previous research; (2) this response, including the strain distribution, is controlled by interactions of slenderness, material properties, and imperfections; and (3) the buckling length (between the points on the bar that represent fixed end conditions) may be considered the controlling length scale for the problem.

Finite Element Simulation

Referring to the preceding sections, the post-peak softening response during both tension necking and compression buckling is controlled by interactive phenomena that are not tractable analytically. However, outcomes of these phenomena (length scales, strain distributions, and softening load-deformation response) are key inputs into the nonlocal uniaxial formulation. To this end, FE simulations discussed in this section parametrically examine these phenomena. Following the structure of the previous section, FE simulations for the necking bar are first described, followed by those for the buckling bar.

Finite Element Simulations of Tensile Necking in a Cylindrical Bar

Finite element models were constructed to simulate the necking response of the cylindrical bar. These may be considered numerical experiments, that is, proxies for experimental response, because

© ASCE

04017091-4

J. Struct. Eng.

they can simulate controlling aspects of behavior (yielding, strain hardening, necking, and the subsequent nonhomogeneous strain field) with accuracy. However, unlike experiments, where data at discrete locations (load and elongation) are usually recovered, FE simulations provide access to the full continuum strain field. The simulations examined two parameters; one is the L/d ratio, whereas the other is a strain-hardening parameter. The former allows examination of the degree to which the localization length is affected by boundary conditions at the ends of the bar. Four values of the L/d ratio were generated by varying the diameter (d_{bar} = 13.5, 16.5, 20, and 25 mm) and holding the length constant (= 200 mm). The material constitutive response was represented as a von Mises material with isotropic hardening. The hardening was represented through the power-law relationship (proposed by Kumar et al. 1981) shown here

$$\sigma = E \cdot \varepsilon \quad \text{for } \sigma \leq \sigma_Y;$$

$$\sigma = \left[\sigma_Y - K \cdot \left(\frac{\sigma_Y}{E} \right)^n \right] + K \cdot \varepsilon^n \quad \text{for } \sigma > \sigma_Y \quad (2)$$

This relationship, which relates the true stress σ to the true strain ε, is defined by three parameters: the yield stress σ_Y and the constants K and n. Of these, two are held constant such that $\sigma_Y = 420$ and $K = 790$ MPa, whereas four values of n (= 0.1, 0.12, 0.15, and 0.18) examine the effect of different rates of strain hardening. The values are consistent with those reported by Kanvinde (2004) for low carbon structural steel. Note that the relationship implied by Eq. (2) reflects a monotonically increasing stress, since it represents continuum response, without geometric nonlinear softening. Along with the parametric variation of the L/d ratio, this results in a total of 16 (= 4 × 4) simulations. For illustrative purposes, Figs. 5(a–d) show the axisymmetric FE model and response for one of these simulations ($d_{bar} = 20$ mm; $n = 0.1$). All models were composed of axisymmetric elements (CAX8R) elements with reduced integration. The mesh was refined to approximately 0.4-mm element size, which is sufficient to capture geometry changes and strain gradients associated with necking. This results in approximately 2,500 elements per model depending on the bar diameter. All models were subjected to displacement controlled tensile loading, as shown in Fig. 5(a). Fig. 5(b) shows the deformed shape in the post-necking phase, whereas Fig. 5(c) shows the engineering stress-strain curve (assuming the gauge length is the length of the model). Referring to Fig. 5(b), the displacement boundary conditions restrict radial deformations at the edge of the model. This radial constraint inhibits plastic flow near the edge, reducing the von Mises stress, and induces necking at the center of the model, without a preexisting imperfection. The magnitude of applied deformations was large enough to produce continuum strains on the order of 1.0 (i.e., 100%) in the necked region, which is on the order of fracture strains in structural steel (Smith et al. 2014), implying that sufficiently large deformations were applied to evaluate the effects of necking. To support the nonlocal formulation, the following quantities were recovered from the simulation: (1) load and deformation over the gauge length of the entire model, including the softening response, as shown in Fig. 5(c); (2) the neck diameter; and (3) the effective uniaxial strain at each longitudinal location along the length of the bar. Parameters and functional forms in the nonlocal formulation were tuned to achieve agreement with these quantities. Recall that although the FE models simulate a 3D response, the nonlocal formulation uses uniaxial longitudinal strain. This uniaxial strain is calculated in two steps. First, an average longitudinal displacement is determined for each cross section based on nodal displacements. Second, the longitudinal displacement field is numerically differentiated to obtain the longitudinal strain field. Fig. 5(d) shows
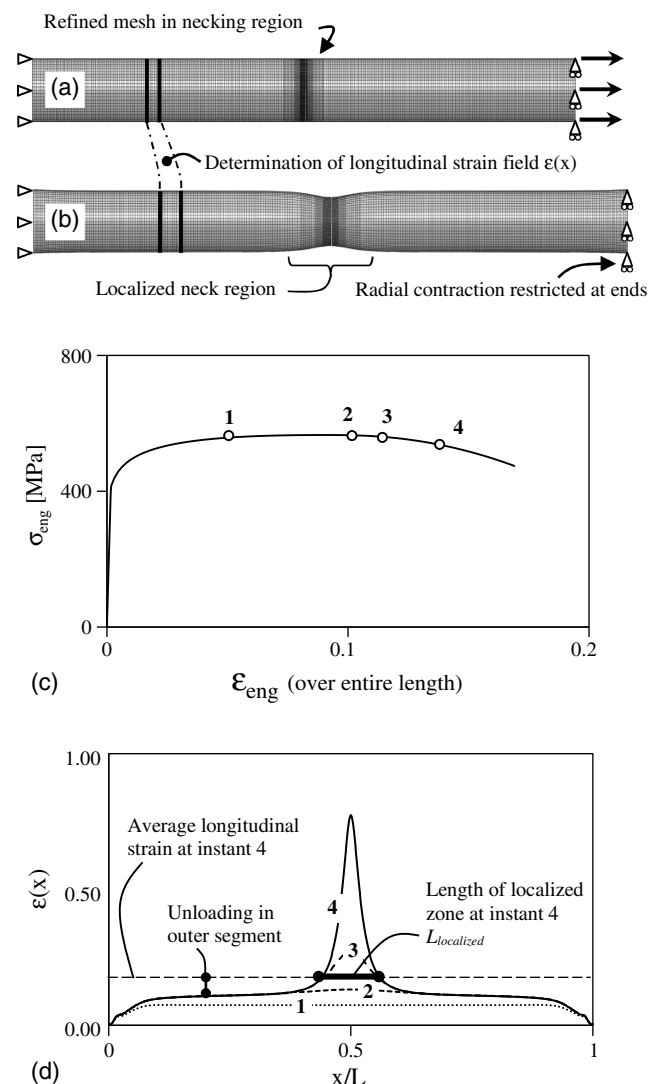

Fig. 5. Finite element simulations for tension bar: (a) undeformed model; (b) deformed model showing neck and strain calculation; (c) engineering stress strain curve; (d) strain field at four loading instants

the evolution of this longitudinal strain field with displacement at four instants during the loading, which are also identified in the load-displacement curve in Fig. 5(c). Referring to these figures, it is noted that:

1. In the initial elastic and hardening phase, the longitudinal strain is uniform over the length of the bar, equal to the applied deformation over the gauge length.
2. Necking initiates at a value of true strain as defined by the Considère criterion [Eq. (1)]. When applied to a power-law material, as is the case here, this results in $\varepsilon_{necking}^{true} = n$, meaning that the true necking strain is numerically equal to the hardening coefficient n [= 0.1 for the simulation shown in Fig. 5; see Marker 2 on Fig. 5(c)].
3. After this point, the strain localizes in the central region of the bar, and the strain outside this region decreases as the material unloads elastically [Fig. 5(d)]. At any instant during this phase of loading, the localized length may be unambiguously defined as the region outside which strain is decreasing at all locations. The localized length provides a measure of the length scale controlling the necking process, for use within the nonlocal formulation.
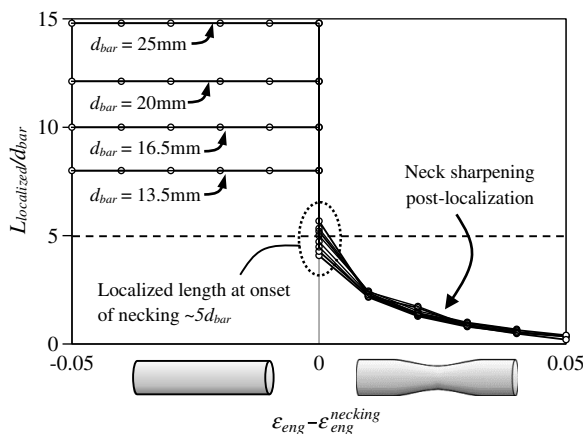
Fig. 6. Evolution of localized length for simulations with different diameters and hardening

Fig. 6 plots the localization length [determined as shown in Fig. 5(d)] against the engineering strain (a measure of deformation over the gauge length) for all 16 simulations. To provide a consistent comparison of post-necking response among the simulations, the horizontal axis is adjusted such that the origin coincides with the strain corresponding to the initiation of necking. Referring to Fig. 6, it is apparent that all simulations, regardless of the hardening coefficient n or d_{bar}, show a virtually coincident evolution of localization length once necking initiates. First, it is interesting to note that the localized length decreases with increasing deformation, indicating that regions that were previously within the neck undergo unloading, forcing the neck to become even sharper. Second, it is noted that immediately after necking, the localized length is approximately five times the diameter of the bar (for all simulations), suggesting a value for the nonlocal formulation.

Finite Element Simulations of Buckling in Prismatic Bar

Finite element simulations were also conducted to simulate buckling in a prismatic bar. In terms of objectives and outputs, they are similar to those for the necking bar (discussed in the previous section). Accordingly, only the distinguishing aspects of these simulations are summarized here. Fig. 7 is analogous to Fig. 5, showing the FE model, the deformed shape, the load-deformation curve, and the projected longitudinal strain distribution. Referring to Fig. 7(a), two-dimensional (2D) models without axisymmetry were constructed to simulate buckling. Eight-node serendipity elements (CPE8R) were used for these models. The models included rotationally fixed boundary conditions at each end and a perturbation applied as a small transverse load at the center to initiate buckling. All models were loaded in compression, so the stress and strain quantities referred to in this section are compressive. Two parameters ($\sigma_y = 280, 420, 500, 600$ MPa; and $L/d = 8, 10, 12,$ and 15) were varied to generate a total of 16 ($= 4 \times 4$) simulations. Fig. 7 shows response of the simulation for $\sigma_y = 420$ MPa and $L/d = 12$. Response of other simulations is qualitatively similar. Referring to Figs. 7(a–d), the main observations are:

1. For the L/d ratios considered in this study, which are consistent with those for buckling rebar, the load deformation curve (unlike that for the necking bar) does not have a plateau but rather abruptly drops from the peak point. It is acknowledged that for material properties and L/d ratios significantly different from
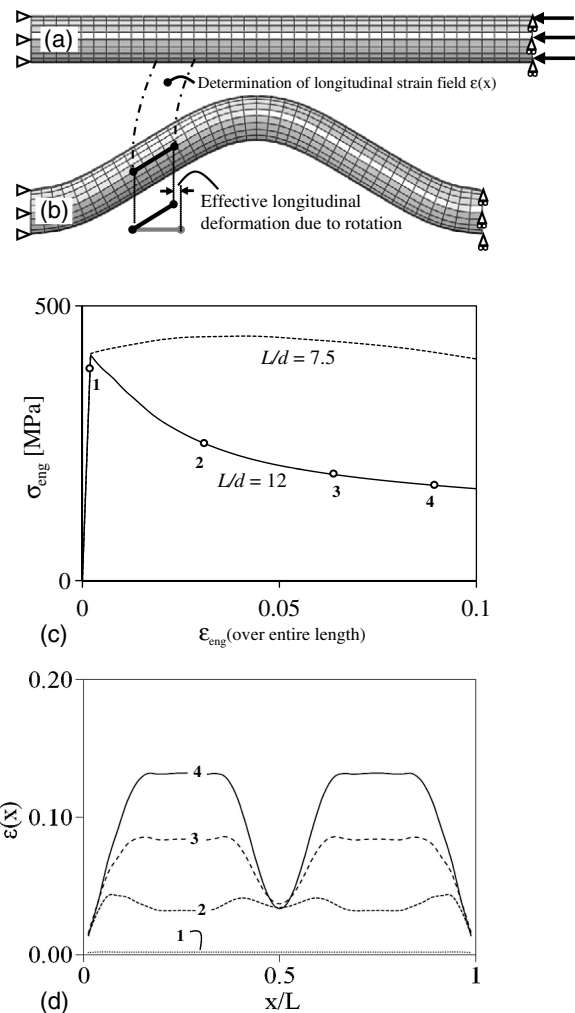

Fig. 7. Finite element simulations for buckling bar with $L/d = 12$: (a) undeformed model for $L/d = 12$; (b) deformed model showing buckling and effective strain; (c) engineering stress strain curve—also shown for $L/d = 7.5$; (d) effective strain field at four loading instants for $L/d = 12$

those used in these simulations the response may be qualitatively different, exhibiting a plateau and even hardening. To illustrate this point, Fig. 7(c) shows the load-deformation curve obtained from a simulation of a buckling bar with $L/d = 7.5$. As is evident from this figure, at this length, the load-deformation curve shows a plateau rather than the sudden drop-off.

2. Referring to Fig. 7(d), the effective longitudinal strain (calculated in a manner similar to the necking bar) is especially interesting considering that two plateaus are observed, along with a low point in the center. A closer evaluation of the underlying kinematics [shown in Figs. 7(a and b)] reveals that in case of the buckling bar, the effective longitudinal strain is a projection of the rotated segments of the bar after buckling rather than axial compression. The nature of this strain field informs the nonlocal formulation for the buckling bar.

Unlike the controlling length scale for the necking bar, which was determined to be dependent on bar diameter and relatively insensitive to boundary conditions, the controlling length scale for the buckling bar is controlled by the boundary conditions. In fact, the simulations indicate that the entire length of the bar between the fixed ends participates in localization, unlike the tension bar where

unloading zones are observed outside the central localized region. Consequently, the formulation is presented assuming that the localization length may be determined a priori, from the boundary conditions in the application scenario of interest. For example, Zong et al. (2014) provide relationships between this length and hoop spacing in a reinforced concrete column. The trends summarized in Figs. 5(a–d) and 6 (for the necking bar) and Figs. 7(a–d) (for the buckling bar) provide a basis for the nonlocal formulation outlined in the next section.

Model Formulation, Implementation, and Results

The nonlocal formulation for both necking and buckling is implemented within a uniaxial, line-element-based structural model through a specially developed *MATLAB* program; this is referred to hereafter as the "line model" to remove ambiguity with respect to the continuum FE model. Fig. 8(a) illustrates the generic line model, Fig. 8(b) shows the constitutive relationships for tension and compression, and Fig. 8(c) outlines the solution process. Multiple variants of this generic model with different meshes, lengths, and loadings (i.e., tension versus compression) were used to develop and validate the nonlocal approach. Referring to Figs. 8(a–c), the line model has the following attributes:

1. Each model represents a bar of length L subdivided into n_{ele} elements, each of length L/n_{ele}. The elements all have a cross-sectional area A, except those selected to have an imperfection, whose area is 0.02% lower as compared to the other elements. Imperfection patterns are discussed separately for the tension and compression formulations. The magnitude of imperfections was selected to be large enough to numerically trigger localization without significantly affecting prelocalization or post-localization response, which was found to be relatively insensitive to imperfection magnitude within a neighborhood of the values used.

2. To examine mesh dependence, multiple n_{ele} are simulated for each parameter set. In all cases, the mesh size is selected such that L/n_{ele} is lower than the characteristic length corresponding to the configuration being simulated, such that the strain field within the localized region is simulated accurately. The nonlocal formulation cannot be interpreted meaningfully if the mesh size is greater than the characteristic length (Wu and Wang 2010).

3. Each element is a constant strain element with linear basis functions without the need for Gauss integration. Consequently, the nonlocal formulation, which requires integration of strains over a neighborhood of a point, directly integrates strains from neighboring elements.

4. For both tension necking and compression buckling, a trilinear constitutive relationship [Fig. 8(b)] is used to represent uniaxial material response. Unlike Eq. (2), which increases monotonically to describe material hardening for the continuum model, the trilinear response includes the softening branch to describe loss of load due to geometric nonlinearity. Furthermore, the trilinear constitutive relationship refers to engineering, rather than true strain. The trilinear relationship is selected because: (1) it is able to functionally represent the load deformation curve, including the softening phase, for both necking and buckling as shown in Fig. 8(b); (2) it is implemented in academic and commercial structural analysis codes such as *OpenSEES* and *LS-DYNA*; and (3) it has relatively few (maximum of five) parameters to calibrate.

The algorithm for the implemented solution is shown in a flowchart [Fig. 8(d)]. Referring to this flowchart, a tangent stiffness matrix based on local strain values and a constitutive model identical to that used for the nonlocal strains is used to determine a trial incremental displacement vector; this greatly facilitates convergence. The local strain values themselves are determined from shape functions applied to the displacement vector from the previous converged load step. Nonlocal strains are then calculated and used within the appropriate constitutive relationship [Fig. 8(b or c)] to determine stresses and conduct force-recovery. A Newton–Raphson iterative scheme is used to eliminate force residuals and
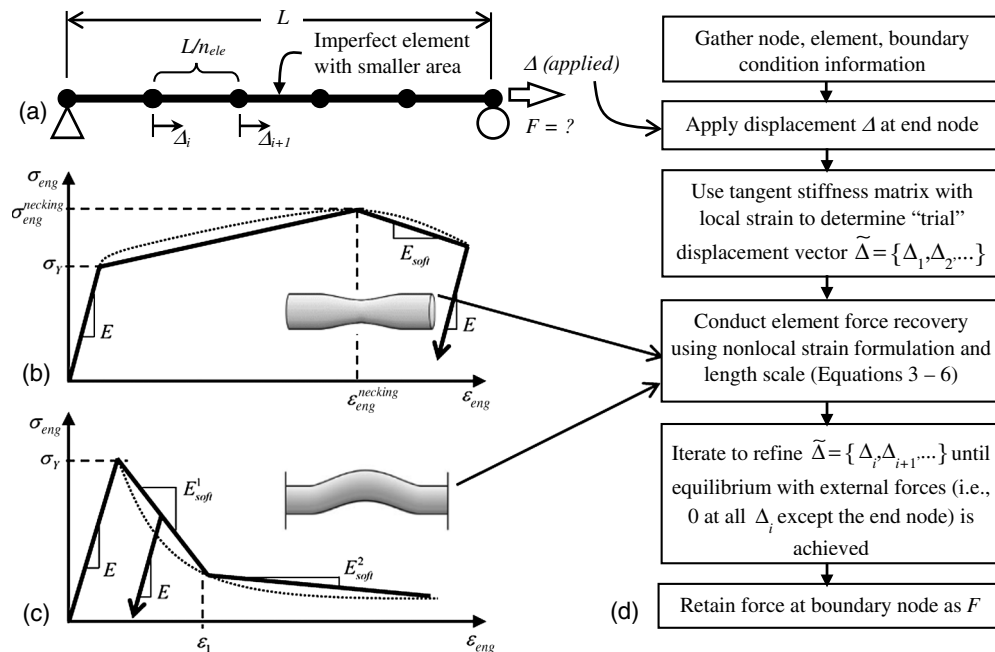

Fig. 8. (a) Generic line model; (b) idealized trilinear constitutive relationship for tension necking; (c) idealized trilinear constitutive relationship for compression buckling; (d) solution process

achieve convergence to a displacement vector. This is retained for the subsequent load step.

Nonlocal Formulation for Necking in Tension Bar

Referring to Fig. 8(b), the constitutive response for necking bar in tension is represented as a trilinear relationship. The first two ascending branches of this relationship describe elastic response followed by strain hardening in a spatially homogeneous manner. The third branch reflects softening, and the introduction of a length scale is necessary to mitigate mesh dependence. Referring to Fig. 8(c), the constitutive relationship utilizes the nonlocal strain measure that incorporates the length scale by averaging strain in the neighborhood of each point. A key feature of the formulation is the development of this strain measure. The formulation is developed with two considerations: mitigation of mesh dependence and simulation of the strain field inside the localized zone. Eqs. (3)–(6) describe the formulation. The nonlocal strain is determined as follows:

$$\varepsilon_p^* = m \cdot \varepsilon_p^w + (1 - m) \cdot \varepsilon_p \qquad (3)$$

In Eq. (3), ε_p^* = nonlocal strain measure used in the constitutive relationship; ε_p^w = weighted average of strain in the neighborhood of any point; ε_p = plastic strain; and m = parameter between 0 and 1. Following the work of Vermeer and Brinkgreve (1994), this is termed an "over-nonlocal" formulation, combining the more basic form of nonlocal strain, which is usually taken directly as ε_p^w, along with the local plastic strain ε_p. This enables a greater degree of control if both the softening load-deformation response as well as the localized strain distribution are targeted. The weighted average strain is determined by integrating the plastic strain over the characteristic length L_c in the neighborhood of each point such that

$$\varepsilon_p^w(x) = \int_{L_c} \alpha(x, \xi) \cdot \varepsilon_p(x, \xi) \cdot d\xi \qquad (4)$$

In Eq. (4), $\alpha(x, \xi)$ = weight function defined over the length L_c; and ξ = local variable with its origin at the material location of interest, that is, x. The weighting function is selected as a bell-shaped function with a peak at x (i.e., at $\xi = 0$), with the following form:

$$\alpha(x, \xi) = \frac{\alpha'(x, \xi)}{\int_{L_c} \alpha'(x, \xi) \cdot d\xi} \qquad (5)$$

where

$$\alpha'(x, \xi) = \frac{15}{8 \cdot L_c} \left[1 - \frac{4 \cdot (x - \xi)^2}{L_c^2} \right] \quad \text{for } |x - \xi|$$
$$\leq L_c/2; \qquad \alpha'(x, \xi) = 0 \quad \text{for } |x - \xi| > L_c/2 \qquad (6)$$

Eq. (5) normalizes the weight function, so it does not alter the nature of a homogeneous strain state. Considering Eqs. (3)–(6), the nonlocal formulation includes two parameters. Of these, m is selected as 0.5 to provide best overall agreement with FE data, and the characteristic length L_c is selected as five times the bar diameter, following the observations of the FE simulations (Fig. 6). Once the strain measure is established in this manner, the constitutive relationship is calibrated in concert with it. Referring to Fig. 8(b) and prior discussion, the first two branches of the trilinear curve correspond to a homogeneous state of strain and, therefore, are unaffected by the gauge length. Accordingly, the parameters associated with these branches (E, σ_Y, $\varepsilon_{\mathrm{eng}}^{\mathrm{necking}}$, $\sigma_{\mathrm{eng}}^{\mathrm{necking}}$) may be determined directly from the true stress-strain curve of the material. For example, the latter two (that is, $\varepsilon_{\mathrm{eng}}^{\mathrm{necking}}$ and $\sigma_{\mathrm{eng}}^{\mathrm{necking}}$), may be determined by applying the Considère criterion to the calibrated constitutive response [Eq. (2)] for the material and subsequently applying transformations to convert the true quantities to their engineering counterparts. The softening branch is controlled by the parameter $E_{\mathrm{soft}} \leq 0$. The unloading stiffness is taken as E [Fig. 8(a)]. Since the formulation is restricted to monotonic loading, laws for reversed cyclic loading (or yielding in the negative direction) are undefined. The softening branch reflects localized, nonhomogeneous strain state. Consequently, its value is sensitive to the gauge length over which it is measured. For consistency with the framework presented, the gauge length for calibration of $E_{\mathrm{soft}} \leq 0$ is taken as $L_c = 5 \cdot d_{\mathrm{bar}}$ (after the observations shown in Fig. 6). This process is used to calibrate the relationship for each of the 16 FE simulations for the necking bar.

Table 1 summarizes the calibrated values of all parameters for each simulation. Once calibrated in this manner, this relationship is used within the line model to reproduce the load deformation response, and the evolution of internal strain distribution for each of the parameter sets examined in the FE simulations. In each line model, the center element is imperfect, with an area 0.02% lower than the other elements.

Figs. 9(a–h) show load deformation curves determined from the line models. These are represented as engineering stress-strain curves, in which the strain is the deformation normalized by the entire length of bar. Before necking, the curves are not dependent on this gauge length. For purposes of illustration, four out of 16 parameter sets (including a range of d_{bar} and n, as indicated on the figures) are selected; results from other parameter sets are qualitatively similar. Figs. 9(a–d) show results from the line model using the local formulation, which is used in conventional fiber models, whereas the figures below them [Figs. 9(e–h)] show counterpart results for the nonlocal formulation. For each figure, results from three levels of mesh discretization are shown along with the corresponding results of the continuum FE simulation. The latter may be considered "true" or objective response. Referring to the figure, it is immediately apparent that for each parameter set the conventional formulation is highly mesh-sensitive such that the finer mesh results in a steeper softening slope. The nonlocal formulation does not show nonobjectivity and closely follows the true or objective response of the continuum FE solution, demonstrating the efficacy of the formulation in mitigating mesh-dependence. In case of the nonlocal formulation, an error is noted between the FE and the structural model solution; this is an artifact of the assumed trilinear constitutive relationship, which cannot perfectly replicate the smooth curve of the FE response.

Figs. 10(a–h) and 11(a–h) are similar to Figs. 9(a–h), except they illustrate other aspects of simulated response. Figs. 10(a–h) indicate the strain distribution along the length of the bar as determined from the local and nonlocal formulations for various mesh sizes and compare it to the objective FE response; these are similar

Table 1. Calibrated Parameters for Uniaxial Constitutive Models for Tension Bar [Fig. 8(b)]

Configuration parameters		Calibrated parameters for uniaxial stress-strain relationship				
L/d	n	E (MPa)	σ_Y (MPa)	$\varepsilon_{\mathrm{eng}}^{\mathrm{necking}}$	$\sigma_{\mathrm{eng}}^{\mathrm{necking}}$ (MPa)	E_{soft} (MPa)
10	0.1	200,000	420	0.105	580	570
10	0.15	200,000	420	0.16	695	360
15	0.1	200,000	420	0.105	580	570
15	0.15	200,000	420	0.16	695	360

Note: $\varepsilon_{\mathrm{eng}}^{\mathrm{necking}} = e^n - 1$, as calculated from the Considère condition.
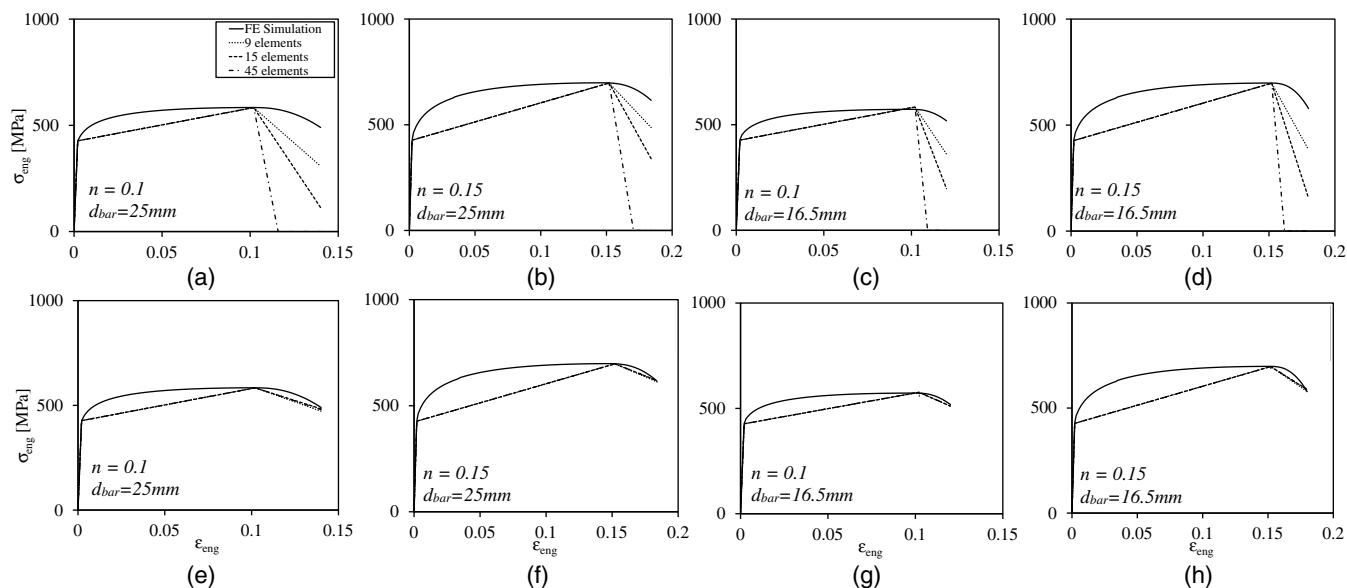
Fig. 9. Engineering stress-strain response for tension bar from FEM and line model (a–d) for local formulation; (e–h) for nonlocal formulation indicating the mitigation of mesh-dependence

to the one shown previously in Fig. 5(d). The strain distributions shown in Figs. 10(a–h) are determined at a deformation 1.25 times the true necking deformation for each parameter set. This deformation (1.25 times necking) was selected because it results in continuum plastic strains on the order of 0.6–0.7 at the center of the necked cross section; these are consistent with the strains required to cause fracture. As a result, the deformations at this point and in Figs. 10(a–h) represent a fully developed localized strain profile. Figs. 11(a–h) show the temporal evolution of longitudinal strain at the center of the bar [similar to the peak point in Fig. 5(d)] determined from the continuum FE model. Note that the engineering strain ε_{eng} plotted on the horizontal axis is a proxy for the axial deformation, normalized across the entire gauge length. Referring to these figures, the following observations may be made:

- All simulations with the local formulation [Figs. 10(a–d)] localize strains in the center element, and the magnitude of this strain varies widely between the different meshes by as much as 300%. This is not surprising, since the model is incapable of distributing strain to adjacent elements, and the center element (with a predetermined length) must accommodate all deformations after localization. Consequently, the strain distributions shown in Figs. 10(a–d) are entirely controlled by element size and are spurious. This means they may not be reliably used for fracture or fatigue prediction. As a result, comparison with the true (FE) strain distribution is of little value.
- Figs. 10(e–h) show response of the nonlocal formulations corresponding to the simulations in Figs. 10(a–d). Referring to these figures, the nonlocal formulation is able to characterize
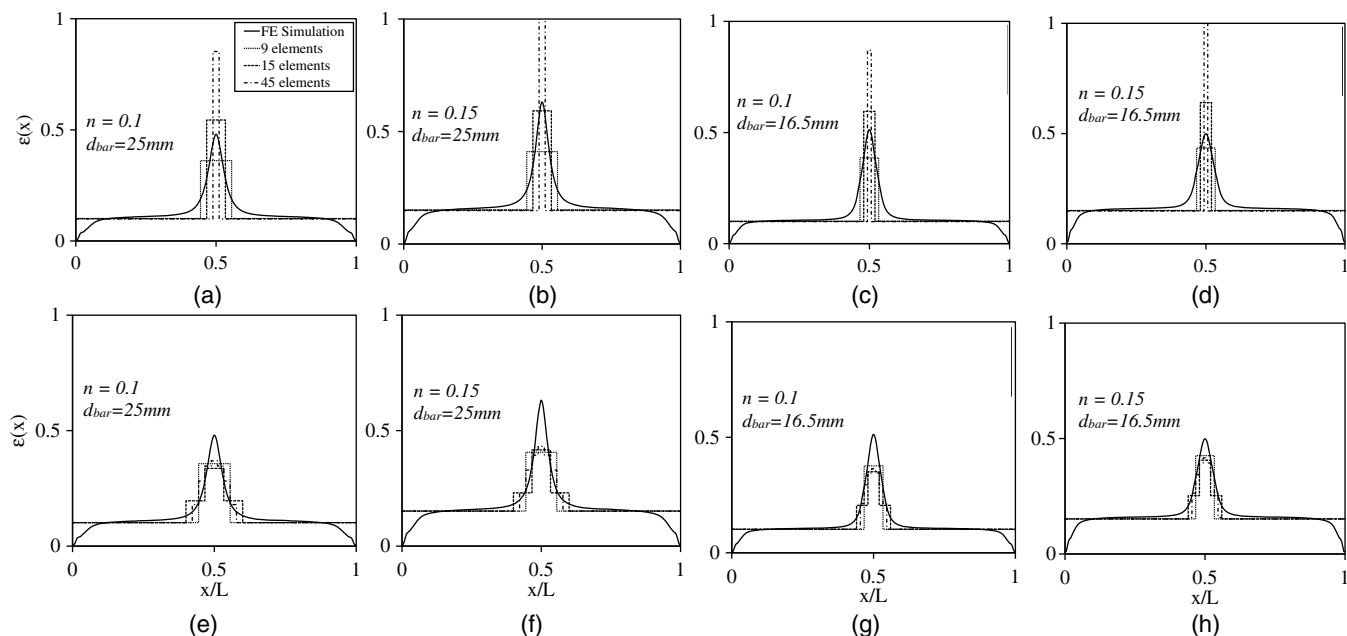

Fig. 10. Longitudinal strain distribution for tension bar from FEM and line model for (a–d) local formulation; (e–h) nonlocal formulation
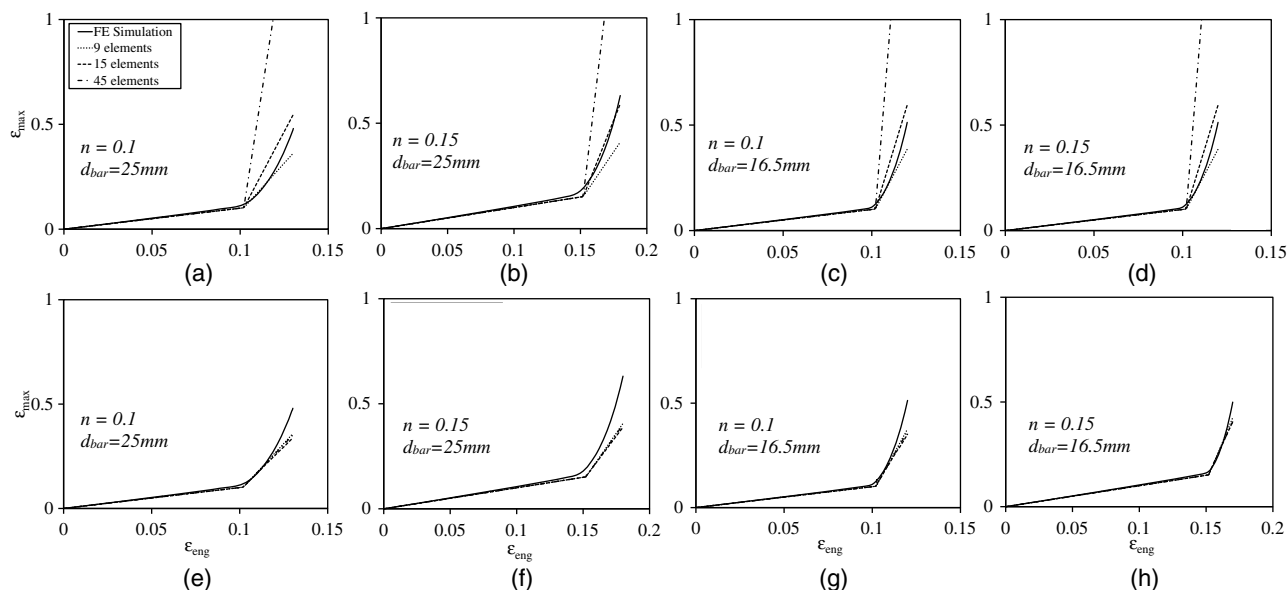
Fig. 11. Evolution of longitudinal strain at the center of the tension bar from FEM and line model for (a–d) local formulation; (e–h) nonlocal formulation

the general nature of the strain distribution by distributing strain to neighboring elements. As the mesh is refined, the distribution approaches the true or objective distribution. However, even in the limit, this does not converge to the true (FE) distribution. This may be attributed to the sharpening of the neck and reduction in localized length (see Fig. 6 and the associated discussion). Since the nonlocal formulation assumes a fixed characteristic length, it cannot capture this second-order aspect of localization. Nonetheless, the formulation mitigates much of the mesh sensitivity of the conventional local formulation. This trend is observed across all 16 parameter sets.

- Referring to Figs. 11(a–h), both local and nonlocal formulations are able to characterize the evolution of peak strain (at the center of the bar) up to the strain at localization. After this point, the strain determined by the local model diverges from the objective (FE) strain, and moreover, the nature of this divergence is highly mesh dependent, such that the finer mesh shows a steeper rise in peak strain. On the other hand, the nonlocal formulation [Figs. 11(e–h)] is able to follow the evolution of the true strain in a mesh independent manner. However, following the point given here, the nonlocal formulation cannot capture the second-order effect of neck sharpening, which produces the nonlinearity in the strain history after localization.

Nonlocal Formulation for Buckling in Compression Bar

Referring to Fig. 8(b), the buckling response of the compression bar is also represented as a trilinear relationship. However, in contrast to the necking bar, the final two branches reflect post-buckling softening, and only the first branch (elastic loading) corresponds to the homogeneous strain state. The double-plateau shape of the effective longitudinal strain for the buckling bar [see Fig. 7(d) and associated discussion] implies that standard nonlocal formulations with a peaked weighting function and central imperfection are incapable of reproducing the strain distribution associated with the buckled bar, albeit they may be used if mesh-independence is the only objective. In an effort to achieve these two objectives simultaneously, the optimal approach to determine nonlocal strains was identical to that used for the tension bar [in terms of weight function form,

and mixed formulation Eqs. (3)–(6)], excepting the following modifications:

1. Initial imperfections with cross-sectional area 0.02% lower than other elements were introduced into two elements located at the 1/4 and 3/4 points along the length. This is in contrast to a single imperfect element at the center of the line models that simulate necking. It is noted here that these imperfections are not physical, but rather notional, to encourage the formation of localized zones at the 1/4 and 3/4 points, resulting in the projected strain distribution that is consistent with the kinematics of the problem [Fig. 7(d)].
2. Following the observations of the FE simulations (the entire length of the bar participates in localized, softening response) and prior discussion, the characteristic length L_c is determined as the distance between the fixed-fixed boundary conditions, that is, $L_c = L$.

The first (elastic) branch of the constitutive relationship may be calibrated through the parameters E and σ_Y, assuming that the compressive strength for this range of L/d ratios is controlled by yielding. Referring to Fig. 8(c), the descending portion of the load deformation curve is approximated by two lines, following the functional form suggested by Zong et al. (2014) that represents reinforcement bar buckling. In these cases too, the unloading relationship for the nonlocal strain is elastic, defined by E [Fig. 8(b)]. Once calibrated in this manner (Table 2), this relationship is used within the line model to simulate response of all 16 parameter sets.

Table 2. Calibrated Parameters for Uniaxial Constitutive Models for Compression Bar [Fig. 8(c)]

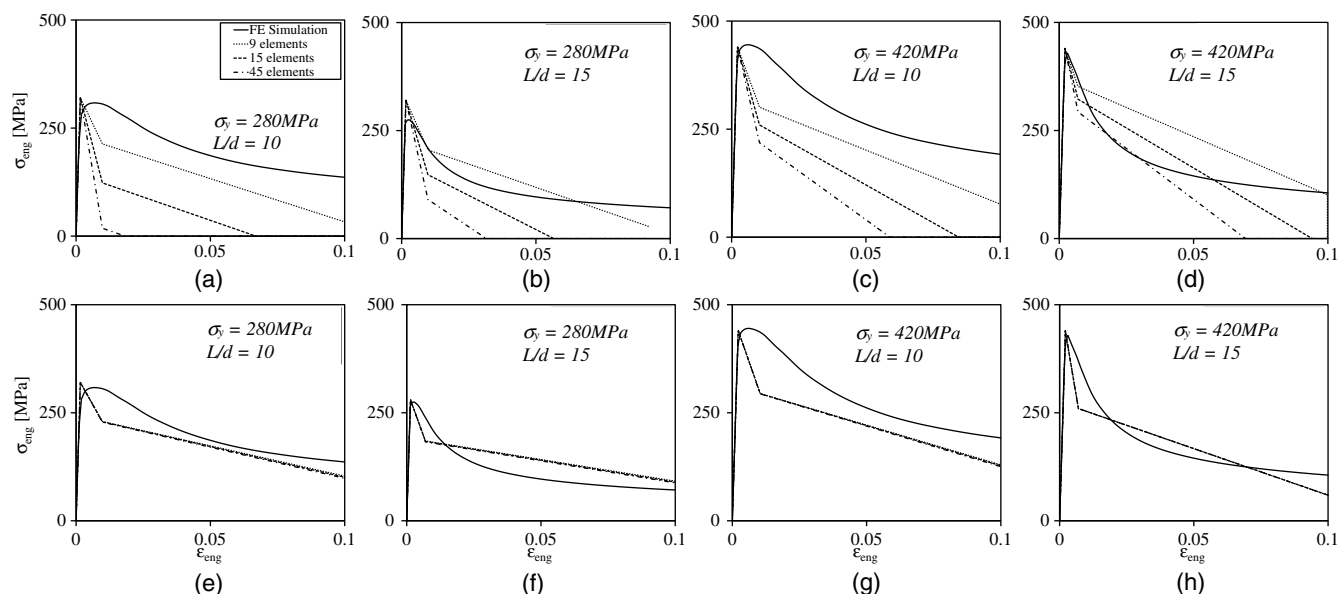| Configuration parameters		Calibrated parameters for uniaxial stress-strain relationship				
L/d	σ_Y	E (MPa)	σ_Y (MPa)	ε_1	E_{soft}^1 (MPa)	E_{soft}^2 (MPa)
10	280	200,000	280	0.0094	11,200	1,440
15	280	200,000	280	0.0056	27,400	1,020
10	420	200,000	420	0.0105	17,850	1,880
15	420	200,000	420	0.0072	36,800	2,150

Fig. 12. Engineering stress-strain response for buckling bars from FEM and line model (a–d) for local formulation; (e–h) for nonlocal formulation indicating the mitigation of mesh-dependence

Figs. 12 and 13 illustrate the simulation results of selected parameter sets. These are analogous to Figs. 9 and 10 shown previously for the necking bar, illustrating the load deformation curve and effective longitudinal strain distribution. Referring to these figures, the following observations may be made:

- Figs. 12(a–d) show engineering stress strain curves (engineering strain is measured over the entire model length) determined from the local formulation, superimposed on the corresponding FE response. As expected, they indicate severe mesh sensitivity in the softening phase, such that the finer mesh results in a steeper softening response.
- Figs. 12(e–h) show that the nonlocal formulation successfully eliminates mesh dependence in load-deformation response, such that the curves are coincident for all element discretizations and for all parameter sets (of which four are shown). However, it is pertinent to note that even the results of the nonlocal formulation

have some error with respect to the objective FE response. This error may be attributed to two factors. First, the softening constitutive response used within the line model [Fig. 8(c)] represents the softening curve only approximately. Second, the softening curve itself, as outlined by Zong et al. (2014), is an empirical fit to true (either FE or experimental response), introducing another layer of inaccuracy. Directly calibrating the constitutive response used in the line model to the FE load deformation data will reduce inaccuracy due to the latter factor. However, the current calibration is retained since it demonstrates efficacy of the approach in the setting in which it is likely to be applied (i.e., using predeveloped functional forms for bar buckling).

- Figs. 13(a–h) show the distribution of longitudinal strain, which represents the post-buckling rotations [Fig. 7(b)], determined at a net compressive engineering strain of 0.1 (10%). Of these, Figs. 13(a–d) suggest that the local formulation is incapable
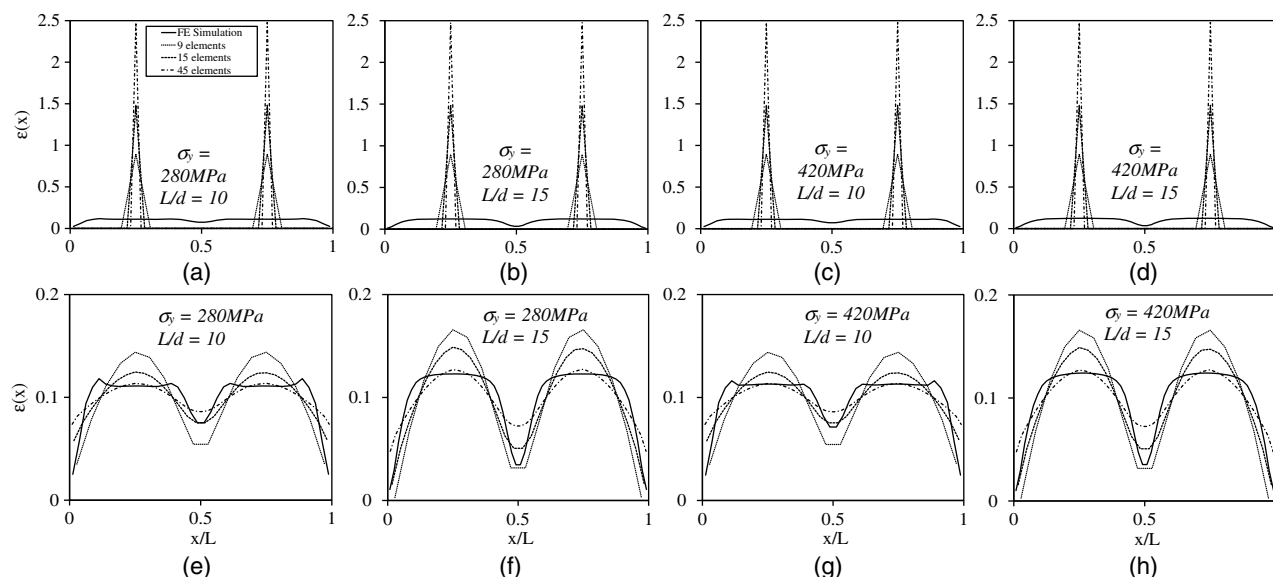

Fig. 13. Longitudinal strain distribution for buckling bars from FEM and line model for (a–d) local formulation; (e–h) nonlocal formulation

of characterizing the strain distribution, concentrating all the strains in the two imperfect elements. This is similar to the phenomenon observed for tension necking in which all strain concentrates in the imperfect central element [Figs. 10(a–d)]. The nonlocal formulation can successfully mitigate this problem by distributing strain to neighboring elements and replicating the FE or true strain distribution qualitatively and even quantitatively, especially as the mesh is refined—compare the solid lines on Figs. 13(e–h) to those representing the curve for 50 elements. This degree of agreement is observed across all parameter sets. Since the longitudinal strain distribution represents post-buckling rotations of bar segments, curves such as the ones shown in Figs. 13(e–h) may be suitably processed to determine bar curvatures and ultimately continuum strains, which may be used to assess fracture or low-cycle fatigue.

Nonlocal formulations are counterintuitive vis-à-vis conventional continuum mechanics since they assume that response at a location is affected by deformation at a remote location. Their philosophical basis requires some elucidation. In the context of material failure, the explanation is that conventional continuum models do not admit the possibility of material heterogeneities that limit localization or otherwise produce interaction between neighboring locations. Following this, aggregate size in concrete or grain size in soils are often a defining length scale in nonlocal models for these materials (Wu and Wang 2010). For the steel bar studied here, nonlocality arises because the uniaxial strain formulation cannot capture the two- or 3D deformations that are responsible for buckling or necking. Thus, nonlocality must be invoked to reintroduce this behavior into the uniaxial construct.

Summary, Conclusions, and Limitations

This article presents a nonlocal formulation that enables simulation of tension necking and compression buckling in a steel bar through line elements using a uniaxial softening constitutive model. In a departure from prior nonlocal formulations which focus on mitigating mesh dependence under material softening, the current formulation addresses localization due to geometric nonlinear effects, and it has the additional objective of simulating strain fields internal to localized zones. The latter is especially important since it enables the assessment of fracture and fatigue directly within a uniaxial fiber-based framework. By incorporating insights gained from continuum FE simulations, the formulation combines efficacy of the FE approach with efficiency of line models. The research focuses on canonical problems of geometric nonlinear localization in tension (necking) and compression (buckling). These problems are attractive because they represent basic forms of localization in steel members. Moreover, the modes of localization and the resulting strain distributions can be simulated directly through FE simulations, providing insights for developing the formulations, as well as a rigorous testbed for validating them. Accordingly, a major research task is continuum FE simulations of necking and buckling bars. While the FE simulation serves to inform and verify the approach, it is noted that such FE simulation is often impractical in the context of building simulations especially when suites of simulation runs must be conducted, such as in seismic collapse fragility analysis (FEMA 2009).

For tension necking, FE simulations reveal that a characteristic length equal to five times the bar diameter controls the localization process. Consequently, the nonlocal formulation uses this length scale. Analogous FE simulations are conducted for compression buckling. These feature a fixed-fixed prismatic bar, in which the length between the fixed ends is determined to be the controlling

characteristic length. For both conditions, the formulations include a nonlocal strain measure with a mixed functional form (combining a local strain with a weighted strain measure), a bell-shaped weight function, and preexisting imperfection locations. These functional forms and weighting methods simultaneously satisfy the objectives of mesh independence while characterizing the localized strain field. The results indicate that these dual objectives are successfully realized across the range of simulation parameters for both the tension and compression scenarios. In summary, the research demonstrates the potential of using nonlocal formulations to simulate geometric nonlinear localization in frame elements.

It is critical to acknowledge that owing to its focus on a simplified problem, the work is of a fundamental nature whose main value lies in demonstrating the adaptation of nonlocal formulations for the purposes outlined here. As a result, the formulation in itself cannot be applied to structural problems with the exception of those that are very similar to the problems examined here in terms of geometry or material properties. The anticipated application of the underlying concepts is in the context of a fiber-type framework for beam-column elements, in which the nonlocal uniaxial model may be used in place of currently used, nonregularized constitutive models to represent local buckling in a cross section or rebar buckling and downstream processes such as fracture. Significant scientific and practical challenges must be overcome before this is accomplished. These include the following:

1. Consideration of force gradients over the localization length: The current formulation is demonstrated only for a constant force over the length of the element. However, in beam-columns with a moment gradient, localization usually occurs under stress gradients along the member axis. The interaction of these stress gradients with localization modes and imperfections is an important future area of study.

2. Investigation of different L/d ratios to examine their influence on post-buckling response: The postbuckling response shown in this paper (i.e., absence of a yield plateau) is not general and may not be valid for L/d ratios that are lower (about 7.5). For these, a different constitutive model (similar to the one used for tensile necking) may be more appropriate.

3. Consideration of cyclic loading: The current formulation assumes tensile and compressive loads to be mutually exclusive. However, in common situations such as seismic loading, elements undergo reversed cyclic loading. Both the material model as well as the nonlocal formulation will require adaptation to successfully simulate these situations. Specifically, history effects pertaining to variable loading amplitudes and unsymmetric cycles must be rigorously considered—even without localization, these issues are challenging in themselves. Kostic et al. (2013) provide discussion of such modeling.

4. Incorporation of single-fiber response into cross-sectional behavior: This research addresses the response of a single element, representative of a fiber within a cross section. Upscaling this response to the cross-section is not trivial and will pose additional challenges. This includes consideration of buckling modes (such as flange or web local buckling) that engage multiple fibers across the cross section and triggering of torsional modes that accompany flexural yielding and softening; see Elkady and Lignos (2015).

5. Implementation within structural analysis code architectures (e.g., OpenSEES): This may not provide convenient functionality for sampling strains from remote locations for stress computations, which is a requisite for the nonlocal formulations.

In summary, major challenges must be overcome to develop the preliminary work presented here into a frame element-based modeling framework that retains the attractive features of fiber

analysis (spread of plasticity, P-M interaction) that is also robust in terms of mesh dependence and provides the opportunity to conveniently incorporate continuum-based fracture and fatigue models within frame elements.

Acknowledgments

References

Armero, F., and Ehrlich, D. (2004). "An analysis of strain localization and wave propagation in plastic beams at failure." *Comput. Meth. Appl. Mech. Eng.*, 193, 3129–3171.

Armero, F., and Ehrlich, D. (2006). "Numerical modeling of softening hinges in thin Euler-Bernoulli beams." *Comput. Struct.*, 84, 641–656.

Bazant, Z. (1976). "Instability, ductility, and size effect in strain-softening concrete." *J. Eng. Mech. Div.*, 102(2), 331–334.

Bridgman, P. W. (1964). *Studies in large plastic flow and fracture*, Harvard University Press, Cambridge, MA.

Coleman, J., and Spacone, E. (2001). "Localization issues in force-based frame elements." *J. Struct. Eng.*, 10.1061/(ASCE)0733-9445(2001)127:11(1257), 1257–1265.

Considère, M. (1885). "Memoirs on the use of iron and steel in construction." *Annales des Ponts et Chaussées*, 9, 574–775.

Dides, M. A., and de la Llera, J. C. (2005). "A comparative study of concentrated plasticity models in dynamic analysis of building structures." *Earthquake Eng. Struct. Dyn.*, 34(8), 1005–1026.

Elkady, A., and Lignos, D. G. (2015). "Analytical investigation of the cyclic behavior and plastic hinge formation in deep wide-flange steel beam-columns." *Bull. Earthquake Eng.*, 13(4), 1097–1118.

Enakoutsa, K., Leblond, J. B., and Perrin, G. (2007). "Numerical implementation and assessment of a phenomenological nonlocal model of ductile rupture." *Comput. Methods Appl. Mech. Eng.*, 196(13), 1946–1957.

Engelen, R. A. B., Geers, M. G. D., and Baaijens, F. P. T. (2003). "Nonlocal implicit gradient enhanced elasto-plasticity for the modeling of softening behavior." *Int. J. Plast.*, 19(4), 403–433.

Faleskog, J., Gao, X., and Shih, C. (1998). "Cell model for nonlinear fracture analysis. I: Micromechanics calibration." *Int. J. Fract.*, 89(4), 355–373.

Fell, B. V. (2008). "Large-scale testing and simulation of earthquake induced ultra low cycle fatigue in bracing members subjected to cyclic inelastic buckling." Ph.D. thesis, Univ. of California, Davis, CA.

Fell, B. V., Kanvinde, A. M., and Deierlein, G. G. (2010). "Large-scale testing and simulation of earthquake induced ultra low cycle fatigue in bracing members subjected to cyclic inelastic buckling." *Technical Rep. 172*, John A. Blume Earthquake Engineering Center, Stanford Univ., Stanford, CA.

FEMA. (2009). *Quantification of building seismic performance factors*, Washington, DC.

Huang, Y. (2009). "Simulating the inelastic seismic behavior of steel braced frames including the effects of low-cycle fatigue." Ph.D. thesis, Univ. of California, Berkeley, CA.

Ibarra, L. F., and Krawinkler, H. (2005). "Global collapse of frame structures under seismic excitations." *Technical Rep. 152*, John A Blume Earthquake Engineering Center, Stanford Univ., Stanford, CA.

Ibrahimbegovic, A. (2009). *Nonlinear solid mechanics: Theoretical formulations and finite element solutions methods*, Springer, New York.

Ikeda, K., and Mahin, S. A. (1986). "Cyclic response of steel braces." *J. Struct. Eng.*, 10.1061/(ASCE)0733-9445(1986)112:2(342), 342–361.

Jin, J., and El-Tawil, S. (2005). "Seismic performance of steel frames with reduced beam section connections." *J. Constr. Steel Res.*, 61(4), 453–471.

Jirásek, M., and Rolshoven, S. (2003). "Comparison of integral-type nonlocal plasticity models for strain-softening materials." *Int. J. Eng. Sci.*, 41(13–14), 1553–1602.

Kanvinde, A. M. (2004). "Micromechanical simulation of earthquake induced fracture in steel structures." *Technical Rep. 145*, John A. Blume Earthquake Engineering Center, Stanford Univ., Stanford, CA.

Kim, K., Bolander, J. E., and Lim, Y. M. (2013). "Failure simulation of RC structures under highly dynamic conditions using random lattice models." *Comput. Struct.*, 125, 127–136.

Kostic, S. M., Filippou, F. C., and Lee, C.-L. (2013). "An efficient beam-column element for inelastic 3D frame analysis." *Computational methods in earthquake engineering*, Vol. 2, Springer, Dordrecht, Netherlands, 49–68.

Krishnan, S., and Hall, J. F. (2006). "Modeling steel frame buildings in three dimensions. I: Panel zone and plastic hinge beam elements." *J. Eng. Mech.*, 10.1061/(ASCE)0733-9399(2006)132:4(345), 345–358.

Kumar, V., German, M. D., and Shih, C. F. (1981). "An engineering approach for elastic-plastic fracture analysis." *NP-1931*, Electric Power Research Institute, Palo Alto, CA.

Lignos, D., and Krawinkler, H. (2011). "Deterioration modeling of steel components in support of collapse prediction of steel moment frames under earthquake loading." *J. Struct. Eng.*, 10.1061/(ASCE)ST.1943-541X.0000376, 1291–1302.

LS-DYNA [Computer software]. Livermore Software Technology Corporation, Livermore, CA.

Marante, M. A., Picon, R., and Florez-Lopez, J. (2004). "Analysis of localization in frame members with plastic hinges." *Int. J. Solids Struct.*, 41, 3961–3975.

MATLAB [Computer software]. MathWorks, Natick, MA.

Needleman, A. (1972). "A numerical study of necking in circular cylindrical bar." *J. Mech. Phys. Solids*, 20(2), 111–127.

NIST (National Institute of Standards and Technology). (2010). "Nonlinear structural analysis for seismic design." *NEHRP Seismic Design Technical Brief No. 4*, NIST, Gaithersburg, MD.

Norris, D. M., Moran, B., Scudder, J. K., and Quiñones, D. F. (1978). "A computer simulation of the tension test." *J. Mech. Phys. Solids*, 26(1), 1–19.

OpenSees [Computer software]. Pacific Earthquake Engineering Research Center, Univ. of California, Berkeley, CA.

Pugh, J. S., Lowes, L. N., and Lehman, D. E. (2015). "Nonlinear line-element modeling of flexural reinforced concrete walls." *Eng. Struct.*, 104, 174–192.

Shuttle, D. A., and Smith, I. M. (1988). "Numerical simulation of shear band formation in soils." *Int. J. Numer. Anal. Methods Geomech.*, 12(6), 611–626.

Sideris, P., and Salehi, M. (2006). "A gradient inelastic flexibility-based frame element formulation." *J. Eng. Mech.*, 10.1061/(ASCE)EM.1943 889.0001083, 04016039.

Smith, C. M., Deierlein, G. G., and Kanvinde, A. M. (2014). "A stress-weighted damage model for ductile fracture initiation in structural steel under cyclic loading and generalized stress states." *Technical Rep. 187*, John A. Blume Earthquake Engineering Center, Stanford Univ., Stanford, CA.

Spacone, E., Filippou, F. C., and Taucer, F. (1996). "Fiber beam-column model for nonlinear analysis of R/C frames. I: Formulation." *Int. J. Earthquake Eng. Struct. Dyn.*, 25(7), 711–725.

Uriz, P. (2005). "Towards earthquake resistant design of concentrically braced steel structures." Ph.D. thesis, Univ. of California, Berkeley, CA.

Valipour, H., and Foster, S. (2009). "Nonlocal damage formulation for a flexibility based frame element." *J. Struct. Eng.*, 10.1061/(ASCE)ST.1943-541X.0000054, 1213–1221.

Vermeer, P. A., and Brinkgreve, R. B. J. (1994). "A new effective non-local strain measure for softening plasticity," *Localization and bifurcation theory for soil and rocks*, A.A. Balkema, Rotterdam, Netherlands, 89–100.

Wu, S., and Wang, X. (2010). "Mesh dependence and nonlocal regularization of one-dimensional strain softening plasticity." *J. Eng. Mech.*, 136(11) 1354–1365.

Zong, Z., Kunnath, S., and Monti, G. (2014). "Material model incorporating buckling of reinforcing bars in RC columns." *J. Struct. Eng.*, 10.1061/(ASCE)ST.1943-541X.0000808, 04013032.